

Energy-based bond graph models of glucose transport with SLC transporters

Weiwei Ai1*, Peter J. Hunter1, and David P. Nickerson1

¹Auckland Bioengineering Institute, University of Auckland, New Zealand

ORIGINAL

Abstract

In Hunter et al. (2025), we proposed an energy-based modelling framework and presented two exemplar bond graph templates for solute carrier (SLC) transporter families: facilitated diffusion with SLC2A2 (GLUT2) and sodium-glucose cotransport with SLC5A1 (SGLT1). In this article, we provide detailed information on the parameterisation process for these two SLC families and the information required to reproduce the results presented in Hunter et al. (2025).

Keywords: SLC transporters, bond graph, energy-based modelling, CellML

Reproducible Model Implementation

http://doi.org/10.17608/physiome.30203617

Primary Publications

P. J. Hunter, W. Ai, and D. P. Nickerson. Energy-based bond graph models of glucose transport with SLC transporters. Biophysical Journal, 124(2):316-335, 2025. ISSN 0006-3495. doi: https://doi.org/10.1016/j.bpj.2024.12.006.

1 Introduction

We presented the bond graph (BG) models for the solute carrier (SLC) family members SLC2A2 and SLC5A1 in Hunter et al. (2025). The models have been implemented using CellML (Cuellar et al., 2003) and the model implementation is available in the Physiome Model Repository (PMR) (Yu et al., 2011) at: https://models.physiomeproject.org/workspace/b65. In that workspace (and in the accompanying OMEX archive) the folders Facilitated transporter and Electrogenic cotransporter hold the models of SLC2A2 and SLC5A1, respectively. Brief descriptions of the CellML model files can be found in the PMR exposure: https://models.physiomeproject.org/e/cd3/. In Sections 3 & 4 we provide detailed introductions to these two exemplar models from Hunter et al. (2025). The instructions for reproducing all the simulation experiments presented in Hunter et al. (2025) are provided in Sections 3.3 & 4.2 for SLC2A2 and SLC5A1, respectively, with instructions on how to initialize these simulation experiments given in section 2.

2 Model and simulation setup

In addition to the CellML models, this study makes use of Python scripts to facilitate simulation and presentation. All files required to reproduce and reuse this study can be obtained by downloading the associated OMEX archive. Alternatively, readers familiar with git may clone the repository at https://models.physiomeproject.org/workspace/b65 using their preferred git client. Please note that as the repository uses git submodules, cloning should be performed recursively. With Git version 2.13 and later, use git clone --recurse-submodules or follow the appropriate instructions based on your Git client.

OPEN ACCESS Reproducible Model

Edited by Rossana Occhipinti

> Curated by Shelley Fong

*Corresponding author

weiwei.ai@auckland.ac.nz

Submitted 2 July 2024

Accepted 29 May 2025

Citation

Ai et al. (2025) Energy-based bond graph models of glucose transport with SLC transporters. Physiome. doi: 10.36903/physiome.30133342

After obtaining the required files, a Python environment with the required capabilities can be created by installing the dependencies listed in the requirements.txt file. This can be done using a command similar to pip install -r requirements.txt or by following the appropriate procedure for the chosen platform.

The src folder contains Python scripts for running simulations, processing simulation results, and plotting data. The primary scripts relevant to this manuscript are summarised here as well as mentioned as they are used in the following sections.

- sim_GLUT2.py: Performs simulations of SLC2A2 and saves the results to </Facilitated transporter/CellMLV2/sim_results>.
- sim_SGLT1.py: Performs simulations of SLC5A1 and saves the results to </Electrogenic cotransporter/CellMLV2/sim_results>.
- mergeData_GLUT2.py: Prepares the data in </Facilitated transporter/CellMLV2/sim_results> for plotting.
- mergeData_SGLT1.py: Prepares the data in </Electrogenic cotransporter/CellMLV2/sim_results> for plotting.
- plot_GLUT2.py: Plots the simulation results for SLC2A2.
- plot_SGLT1.py: Plots the simulation results for SLC5A1.

Other Python scripts were used to generate the SED-ML files in </Facilitated transporter/CellMLV2/> and </Electrogenic cotransporter/CellMLV2/>. These SED-ML files are provided so users do not need to run the scripts again.

3 SLC2A2 bond graph model parameterisation

The SLC2A2 (protein name GLUT2) uses the extracellular to intracellular glucose concentration gradient to drive transmembrane transport of glucose in a process called 'facilitated diffusion', and we replicated the bond graph diagram in Figure 1 for convenience. The kinetic data that we used to obtain the parameters of the bond graph model were from Lowe and Walmsley (1986), and the kinetic model diagram is shown in Figure 2. Note that the notation and the parameter names in the kinetic diagram are different from the bond graph. Additionally, the bond graph model of SLC2A2 can be generalised and parameterised to represent any member of the SLC2 family. The data from Lowe and Walmsley (1986) were measured for SLC2A1/GLUT1, while SLC2A2/GLUT2 is used in this Physiome paper to remain consistent with the primary reference Hunter et al. (2025).

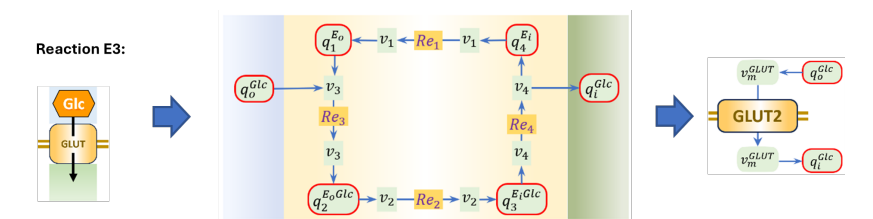


Figure 1. Bond graph of SLC2A2, replicated from Hunter et al. (2025).

Table 1 lists the kinetic parameters, which are the rate constants associated with the forward and reverse reaction fluxes in the traditional mass-action equations. The first column of Table 1 is the corresponding parameter names for the reactions in the bond graph where the subscript indicates the reaction number, while the second column lists the kinetic parameter names in Lowe and Walmsley (1986).

3.1 Bond graph parameters

Pan (2019) introduced a method to convert kinetic parameters to bond graph parameters provided that the kinetic models are thermodynamically consistent. Here, we use the SLC2A2 example

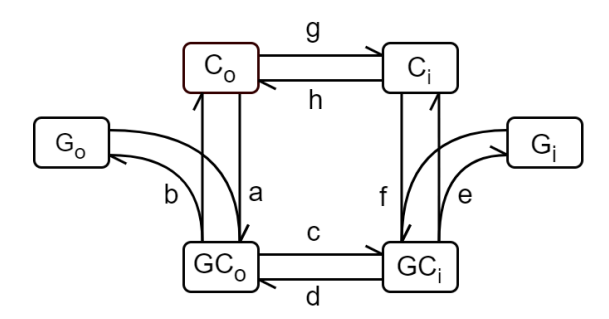


Figure 2. Kinetic model diagram adapted from Lowe and Walmsley (1986). Note that the notations for the conformation states of the transporter are different from the bond graph: $C_o - E_o(BG)$; $C_i - E_i(BG)$; $G_o - E_oGlc(BG)$; $G_i - E_iGlc(BG)$; $G_o - Glc_o(BG)$; $G_i - Glc_o(BG)$. The letters associated with the edges are the rate constants and the arrows indicate the flux directions.

Table 1. The kinetic parameters in Lowe and Walmsley (19	₹86).
---	-------

Kinetic in BG	Parameter in Lowe and Walmsley (1986)	Value	Unit
k_1^+	h	0.726	s^{-1}
k_2^+	С	1113	s^{-1}
k_3^{+}	а	4.5e7 ¹	$mM^{-1}.s^{-1}$
k_4^+	e	$2.7e5 \times 12.8459^{-2}$	s^{-1}
k_1^{-}	g	12.1	s^{-1}
k_2^-	d	90.3	s^{-1}
k_{3}^{-}	Ь	$4.5e7 \times 9.5^{3}$	s^{-1}
k_4^-	f	2.7e5 ¹	$mM^{-1}.s^{-1}$

¹ Not given in Lowe and Walmsley (1986), we use a large number to align with the fast binding assumption (Lowe and Walmsley, 1986; Hunter et al., 2025).

to detail the link between the kinetic parameters in traditional mass-action equations and bond graph parameters. In particular, kinetic models often capture the fluxes J using the unit such as $mM.s^{-1}$, while bond graph usually explicitly models the flow rate v using the unit such as $f mol.s^{-1}$ and potentials μ using the unit $J.mol^{-1}$ for biochemical reactions. When we convert the kinetic parameters to bond graph parameters, we need to consider such dimensional differences.

Conventionally, the rate of biochemical reactions can be described by the law of mass action. The rate of the forward reaction J^+ ($mM.s^{-1}$) (also known as forward flux) is proportional to the amount of the reactants (E, as shown in Equation 1), while the rate of the reverse reaction J^- ($mM.s^{-1}$) (also known as reverse flux) is proportional to the amount of the products (P, as shown in Equation 2). $[C_i]$ (mM) and $[C_j]$ (mM) are the concentrations of reactants and products, k^+ and k^- are the forward and reverse rate constants, while v_i^f and v_j^r are the corresponding stoichiometric coefficients.

$$J^{+} = k^{+} \prod_{i \in E} [C_{i}]^{v_{i}^{f}}$$
 (1)

$$J^{-} = k^{-} \prod_{j \in P} [C_j]^{v_j^r}$$
 (2)

The total rate of reaction J ($mM.s^{-1}$) (i.e., net flux) is expressed in Equation 3.

² Apply the constraint e/f = 12.8459 (mM).

³ Apply the constraint b/a = 9.5 (mM)

$$J = J^{+} - J^{-} = k^{+} \prod_{i \in E} [C_{i}]^{v_{i}^{f}} - k^{-} \prod_{j \in P} [C_{j}]^{v_{j}^{f}}$$
(3)

In the case of the reaction network of SLC2A2 (Figure 1), we can express the fluxes using Equation 4.

$$\mathbf{J} = \begin{bmatrix} J_1 \\ J_2 \\ J_3 \\ J_4 \end{bmatrix} = \begin{bmatrix} k_1^+ [C_4] - k_1^- [C_1] \\ k_2^+ [C_2] - k_2^- [C_3] \\ k_3^+ [C_1] [C_{Ao}] - k_3^- [C_2] \\ k_4^+ [C_3] - k_4^- [C_4] [C_{Ai}] \end{bmatrix}$$
(4)

The bond graph formulation highlights thermodynamic consistency and the flow of chemical species is driven by the chemical potentials (Pan, 2019). The chemical potential μ_i of a specicies i is determined by the molar amount of q_i (f mol), shown in Equation 5, where R = 8.314 ($J.K^{-1}.mol^{-1}$) is the ideal gas constant, T (K) is the absolute temperature and K_i (f mol^{-1}) is the thermodynamic constant of the species.

$$\mu_i = RTIn(K_i q_i) \tag{5}$$

The rate of a reaction v_R ($fmol.s^{-1}$) can be expressed using the Marcelin-de Donder equation (Equation 6). A_R^f ($J.mol^{-1}$) is the forward affinity (the total chemical potential of the reactants) and A_R^r ($J.mol^{-1}$) is the reverse affinity (the total chemical potential of the products).

$$v_R = \kappa (e^{A_R^f/RT} - e^{A_R^r/RT}) \tag{6}$$

For example, the flow rate of the reaction Re₃ in Figure 1 can be given by Equations 7, 8 and 9.

$$v_3 = \kappa_3 (e^{A_3^f/RT} - e^{A_3^f/RT}) \tag{7}$$

$$A_3^f = \mu_1 + \mu_{Ao} = RT \ln(K_1 q_1) + RT \ln(K_{Ao} q_{Ao})$$
 (8)

$$A_3^r = \mu_2 = RTIn(K_2 q_2) \tag{9}$$

Equation 7 can be rearranged as Equation 10 by substituting Equations 8 and 9 into Equations 7.

$$v_3 = \kappa_3 K_1 K_{Ao} q_1 q_{Ao} - \kappa_3 K_2 q_2 \tag{10}$$

The flow rates of the reaction network of SLC2A2 (Figure 1), can be expressed using Equation 11.

$$\mathbf{v} = \begin{bmatrix} v_1 \\ v_2 \\ v_3 \\ v_4 \end{bmatrix} = \begin{bmatrix} \kappa_1 K_4 q_4 - \kappa_1 K_1 q_1 \\ \kappa_2 K_2 q_2 - \kappa_2 K_3 q_3 \\ \kappa_3 K_1 K_{AO} q_1 q_{AO} - \kappa_3 K_2 q_2 \\ \kappa_4 K_3 q_3 - \kappa_4 K_4 K_{Ai} q_4 q_{Ai} \end{bmatrix}$$
(11)

The relationship between the molar amount q_i (fmol) and the concentration $[C_i]$ (mM) of a species is $q_i = [C_i]V_i$, where V_i (pL) is the volume of the compartment in which the species resides. Equation 11 can be rewritten as Equation 12 if we incorporate the concentrations of species rather than the molar amount.

$$\mathbf{v} = \begin{bmatrix} v_1 \\ v_2 \\ v_3 \\ v_4 \end{bmatrix} = \begin{bmatrix} \kappa_1 K_4 V_4 [C_4] - \kappa_1 K_1 V_1 [C_1] \\ \kappa_2 K_2 V_2 [C_2] - \kappa_2 K_3 V_3 [C_3] \\ \kappa_3 K_1 V_1 K_{Ao} V_{Ao} [C_1] [C_{Ao}] - \kappa_3 K_2 V_2 [C_2] \\ \kappa_4 K_3 V_3 [C_3] - \kappa_4 K_4 V_4 K_{Ai} V_{Ai} [C_4] [C_{Ai}] \end{bmatrix}$$
(12)

By comparing Equations 4 and 12, we can see the relationship between the kinetic parameters (k^+, k^-) and the bond graph parameters (κ, K) :

$$\begin{bmatrix}
k_1^+ \\ k_2^+ \\ k_3^+ \\ k_4^- \\ k_1^- \\ k_2^- \\ k_3^- \\ k_4^- \end{bmatrix} = \begin{bmatrix}
\kappa_1 K_4 V_4 \\ \kappa_2 K_2 V_2 \\ \kappa_3 K_1 V_1 K_{Ao} V_0 \\ \kappa_4 K_3 V_3 \\ \kappa_1 K_1 V_1 \\ \kappa_2 K_3 V_3 \\ \kappa_3 K_2 V_2 \\ \kappa_4 K_4 V_4 K_{Ai} V_i
\end{bmatrix}$$
(13)

By defining **Ln** as an element-wise logarithm operator, Equation 13 can be linearized and rewritten as the matrix equation:

In Pan (2019), the above equation was generalised using Equation 15.

$$Ln(k) = MLn(W\lambda) \tag{15}$$

where

$$\mathbf{k} = \begin{bmatrix} k^{+} \\ k^{-} \\ K^{c} \end{bmatrix}, \ \mathbf{M} = \begin{bmatrix} I_{n_{r} \times n_{r}} & N^{fT} \\ I_{n_{r} \times n_{r}} & N^{rT} \\ 0 & N^{cT} \end{bmatrix}, \ \lambda = \begin{bmatrix} \kappa \\ K \end{bmatrix}.$$
 (16)

 $I_{n_r \times n_r}$ is an identity matrix of length n_r , while n_r is the number of reactions. N^{fT} and N^{rT} are the transpose of forward and reverse stoichiometric matrices N^f and N^r , respectively. The vectors

Table 2. Forward stoichiometric matrix N^f for the SLC2A2.

	Re_1	Re_2	Re_3	Re_4
Ai	0	0	0	0
Ao	0	0	1	0
1	0	0	1	0
2	0	1	0	0
3	0	0	0	1
4	1	0	0	0

Table 3. Reverse stoichiometric matrix N^r for the SLC2A2.

	Re_1	Re_2	Re_3	Re_4
Ai	0	0	0	1
Ao	0	0	0	0
1	1	0	0	0
2	0	0	1	0
3	0	1	0	0
4	0	0	0	1

of the forward and reverse kinetic rate constants k^+ , k^- , and the vector of known constraints K^c between the species defined in the matrix N^c for SLC2A2 are shown in Equation 17.

$$\mathbf{k}^{+} = \begin{bmatrix} k_{1}^{+} \\ k_{2}^{+} \\ k_{3}^{+} \\ k_{4}^{+} \end{bmatrix}, \ \mathbf{k}^{-} = \begin{bmatrix} k_{1}^{-} \\ k_{2}^{-} \\ k_{3}^{-} \\ k_{4}^{-} \end{bmatrix}, \ \mathcal{K}^{c} = [], \ \mathbf{N}^{c} = []$$
(17)

The orders of the elements in \mathbf{k}^+ and \mathbf{k}^- are the same order of the reactions, organized as columns in the matrices N^f and N^r , shown in Table 2 and Table 3, while N^c is organized by [number of species]×[number of K^c]. Note that we do not need to add constraints in this case therefore both K^c and N^c are empty.

The diagonal matrix **W** (Equation 18) accounts for the volumes of compartments and the size is 10 ([number of reactions]+[number of species]). The typical blood cell volume $V_i = 0.09$ (pL) according to McLaren et al. (1987) and we set the extracellular volume $V_o = 0.09$ (pL) as well. Since the protein SLC2A2 does not exist in a compartment, we set volumes of corresponding conformations of the protein $V_1 = V_2 = V_3 = V_4 = 1$ (pL) (Pan, 2019). That is, their thermodynamic constants are not related to the volumes.

Given the above vectors and matrices, we can obtain bond graph parameters λ by matrix inversion (Equation 19),

$$\lambda_0 = \mathbf{W}^{-1} \mathbf{Exp}(\mathbf{M}^+ \mathbf{Ln}(\mathbf{k})) \tag{19}$$

Table 4. The bond graph parameters of the full BG model for SLC2A2.

Parameter	Value	Unit
<u>κ</u> 1	0.36	fmol.s ⁻¹
κ_2	0.26	$fmol.s^{-1}$
<i>K</i> ₃	1.01E+05	$fmol.s^{-1}$
κ_4	1.01E+04	$fmol.s^{-1}$
$egin{aligned} \mathcal{K}_i^A \ \mathcal{K}_o^A \end{aligned}$	149.65	$f mol^{-1}$
K_o^A	149.65	$f mol^{-1}$
<i>K</i> ₁	33.2	$f mol^{-1}$
K_2	4.25E+03	$f mol^{-1}$
K_3	344.59	$f mol^{-1}$
<i>K</i> ₄	1.99	f mol⁻¹

where M^+ is the Moore-Penrose pseudoinverse of M and Exp is the element-wise exponential. The resulting bond graph parameters based on Equation 19 are shown in Table 4.

3.2 Parameters for steady state

Hunter et al. (2025) provided the analytical expression in Equation 20 (Hunter et al., 2025) to calculate the parameters for the steady-state flux in Equation 19 (Hunter et al., 2025) using the bond graph parameters in Table 4. We refer the readers to the primary paper for the analytical derivation process and calculation, while we explain here how we obtained the parameters from the steady-state data (Lowe and Walmsley, 1986).

The Michaelis-Menten formulation of zero trans influx (Lowe and Walmsley, 1986) of the transporter, i.e., set the intracellular concentration to be 0 (mM), is shown in Equation 20,

$$V_{oi} = V_{oi}^{max} \frac{[A]_o}{K_{oi} + [A]_o} (mM.s^{-1})$$
(20)

where $[A]_o$ is the extracellular concentration of glucose, the maximum flux V_{oi}^{max} is calculated using Equation 21 with the concentration of glucose carrier molecules [C] in human red blood cells of 6.67 (μM) (Lowe and Walmsley, 1986).

$$V_{oi}^{max} = \frac{[C]}{1/c + 1/h} = 0.0048 \ (mM.s^{-1})$$
 (21)

The Michaelis-Menten constant of Equation 20 is calculated using Equation 22 (Lowe and Walmsley, 1986), where $\frac{b}{a}$ is the dissociation constant of reaction Re_3 .

$$K_{oi} = \frac{b}{a} \frac{1 + g/h}{1 + c/h} = 0.1094 \ (mM)$$
 (22)

When the intracellular molar amount of glucose is zero, the steady-state expression (Equation 19 in Hunter et al. (2025)) can be rearranged to Equation 23.

$$v_{oi} = \frac{k_m^1 v_m q_o^A}{\frac{k_m^1}{K_o^A} + q_o^A} (f mol. s^{-1})$$
 (23)

Substitute q_o^A in the above equation with $[A]_oV_o$, and add the $V_E = 1$ (pL) term to convert the unit from $f mol.s^{-1}$ to $mM.s^{-1}$ and rearrange it to Equation 24.

$$v_{oi}^{mm} = k_m^1 v_m / V_E \frac{[A]_o}{\frac{k_m^1}{K_o^A V_o} + [A]_o}$$
 (24)

We obtain the following relationships in Equations 25 and 26 by comparing Equations 20 and 24.

$$K_{io} = \frac{k_m^1}{K_o^A V_o} \tag{25}$$

$$V_{oi}^{max} = k_m^1 v_m / V_E \tag{26}$$

Hence, we obtained the parameters k_m^1 and v_m using Equations 27 and 28.

$$k_m^1 = K_{oi} K_o^A V_o = 1.4735 (27)$$

$$v_m = V_{oi}^{max} * V_E/k_m^1 = 0.003284 \ (f \, mol. s^{-1})$$
 (28)

The Michaelis-Menten of zero trans efflux (Lowe and Walmsley, 1986) i.e., set the extracellular concentration to be $0 \ (mM)$, is shown in Equation 29.

$$V_{io} = V_{io}^{max} \frac{[A]_i}{K_{io} + [A]_i} (mM.s^{-1})$$
(29)

, where $[A_i]$ is the intracellular concentration of glucose, and the maximum flux V_{io}^{max} is calculated using Equation 30 (Lowe and Walmsley, 1986).

$$V_{io}^{max} = \frac{[C]}{1/d + 1/g} = 0.0712 \ (mM.s^{-1})$$
 (30)

The Michaelis-Menten constant is calculated using Equation 31 (Lowe and Walmsley, 1986), where $\frac{e}{f}$ is the dissociation constant of reaction Re_4 .

$$K_{io} = \frac{e}{f} \frac{1 + h/g}{1 + d/g} = 1.609 \ (mM) \tag{31}$$

When the extracellular molar amount of glucose is zero, the steady-state expression (Equation 19 in Hunter et al. (2025)) can be rearranged to Equation 32.

$$v_{io} = -\frac{k_m^2 v_m q_i^A}{\frac{k_m^2}{K_i^A} + q_i^A} (f \, mol. s^{-1})$$
(32)

Substitute q_i^A in the above equation with $[A]_i V_i$, and add the $V_E = 1$ (pL) term to convert the unit from $f mol.s^{-1}$ to $mM.s^{-1}$ and rearrange it to Equation 33.

$$v_{io}^{mm} = k_m^2 v_m / V_E \frac{[A]_i}{\frac{k_m^2}{K^A V_i} + [A]_i}$$
(33)

By comparing Equations 29 and 33, we obtained Equation 34.

$$V_{io}^{max} = k_m^2 v_m / V_E \tag{34}$$

Then we can calculate the parameter k_m^2 using Equation 35.

$$k_m^2 = V_{io}^{max} * V_E / v_m = 21.671$$
 (35)

 k_m^3 is calculated using Equation 20 in Hunter et al. (2025). The parameters are summarized in Table 5.

Table 5. The parameters of the steady state bond graph model for SLC2A2.

Parameter	Value	Unit
v _m	0.003284	$fmol.s^{-1}$
k_m^1	1.4735	dimensionless
k_m^2	21.671	dimensionless
k_m^3	235.07	dimensionless

Table 6. Summary of the model files, parameters and corresponding simulation plots in Figure 3

Model file	Parameters	Plot in Figure 3
GLUT2_kinetic.cellml	Table 1	Lowe AG and Walmsley AR (1986) in Figure 3 (a) and (b)
GLUT2_BG.cellml	Table 4	Bond graph in Figure 3 (a) and (b)
GLUT2_ss_oi.cellml	Table 4 for Steady-state	Steady-state Eq. 19 and Steady-state Eqs
	Eqs 19 and 20 and Table 5 for Steady-state Eq. 19	19 and 20 in Figure 3 (a)
GLUT2_ss_io.cellml	Table 4 for Steady-state	Steady-state Eq. 19 and Steady-state Eqs
	Eqs 19 and 20 and Table	19 and 20 in Figure 3 (b)
	5 for Steady-state Eq. 19	

3.3 Simulation results

We encoded the full bond graph model (Hunter et al., 2025) in *GLUT2_BG.cellml* and the parameters in *params_BG.cellml*. To simulate the inward flux, we set the molar amount of intracellular glucose q_{Ai} to be a very small value 0.09e - 4 (fmol), and varied the molar amount of extracellular glucose q_{Ao} from 0.09e - 4 (fmol) to 2.25 (fmol). For each extracellular glucose value, we simulate the model for 250 seconds to get the steady-state flow rate. Similarly to simulate the outward flux, we set the molar amount of extracellular glucose q_{Ao} to be a very small value 0.09e - 4 (fmol), and varied the molar amount of intracellular glucose q_{Ai} from 0.09e - 4 (fmol) to 2.25 (fmol). For each intracellular glucose value, we simulate the model for 250 seconds to get the steady-state flow rate.

We encoded the Equations 20 and 29 in $GLUT2_kinetic.cellml$ and simulated the zero trans influx and efflux by varying the extracellular glucose concentration and intracellular glucose concentration respectively from $1e - 8 \ (mM)$ to $25 \ (mM)$.

The steady-state model in Equations 19 and 20 in Hunter et al. (2025) were encoded in $GLUT2_ss_oi.cellml$ and $GLUT2_ss_oi.cellml$. $GLUT2_ss_oi.cellml$ sets the molar amount of intracellular glucose q_{Ai} to be very small value 0.09e - 8 (fmol) and varies the molar amount of extracellular glucose q_{Ao} from 0.09e - 8 (fmol) to 2.25 (fmol); $GLUT2_ss_oi.cellml$ sets the molar amount of extracellular glucose q_{Ao} to be very small value 0.09e - 8 (fmol) and varies the molar amount of intracellular glucose q_{Ai} from 0.09e - 8 (fmol) to 2.25 (fmol).

Figure 3 shows the steady-state fluxes from the full bond graph model and steady-state model in Hunter et al. (2025) compared to the zero trans influx (Equation 20) and efflux (Equation 29) in Lowe and Walmsley (1986). The plots in red used the parameters in Table 5 for Equation 19 in Hunter et al. (2025), while the magenta lines used the parameters in Table 4 to calculate the parameters for Equation 19 in Hunter et al. (2025) according to Equation 20 in Hunter et al. (2025).

We summarize the models, parameters, and corresponding simulation plots in Table 6. We have provided the Python scripts under the folder <src> to run the simulations and plot the data, while the SED-ML files in <Facilitated transporter\CellMLV2> detail the simulation settings. To get the result in Figure 3, the Python scripts $sim_GLUT2.py$, $mergeData_GLUT2.py$, $plot_GLUT2.py$ should run in sequence.

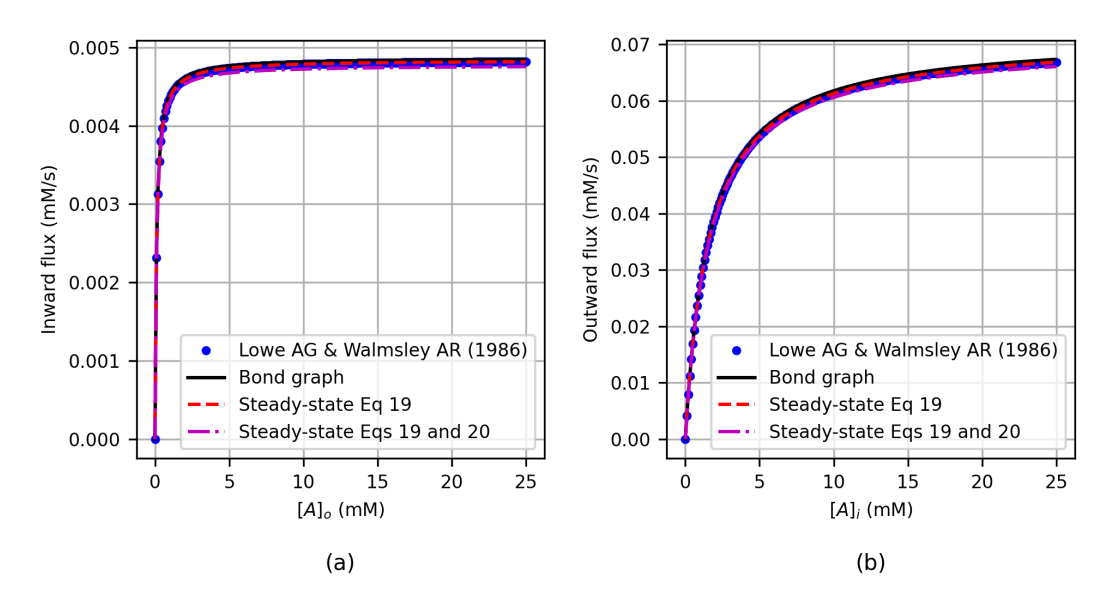


Figure 3. (a) Inward flux as a function of $[A]_o$ when $[A]_i = 0$, and (b) outward flux as a function of of $[A]_i$ when $[A]_o = 0$. Note that in order to compare with the kinetic data in Lowe and Walmsley (1986), the molar amount of glucose in the bond graph model was converted to glucose concentrations. This is Figure 8 in Hunter et al. (2025).

4 SLC5A1 bond graph model parameterization

The SLC5A1 (SGLT1) uses the sodium gradient to drive glucose into the cell, typically when the transmembrane glucose gradient is insufficient to provide the required flux of glucose. The bond graph is shown in Figure 4. We parameterize the bond graph model to fit the data in Parent et al. (1992), and the kinetic model diagram is shown in Figure 5. Note that the notation and the parameter names in the kinetic diagram are different from the bond graph.

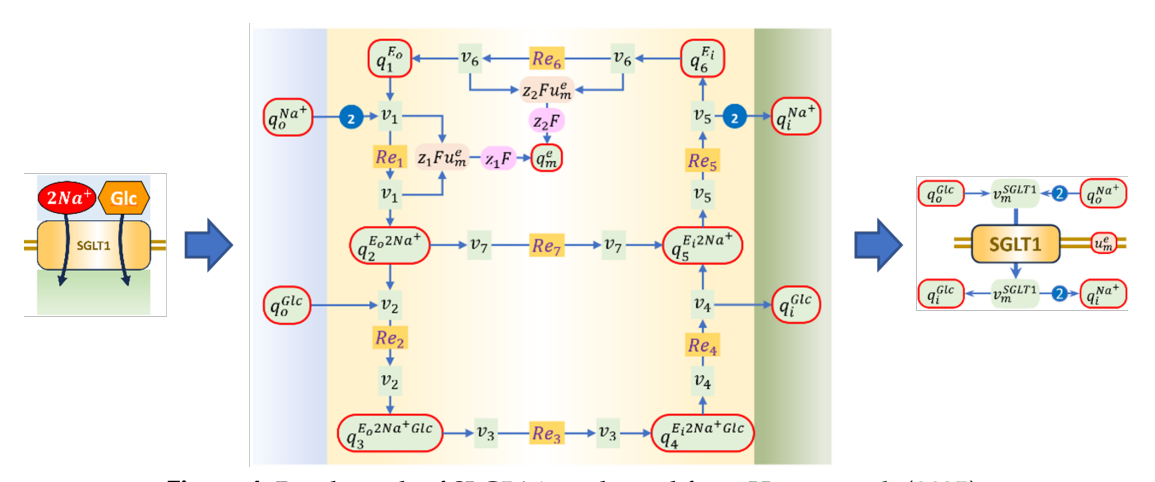


Figure 4. Bond graph of SLC5A1, replicated from Hunter et al. (2025).

The kinetic parameters in in Parent et al. (1992) are listed in Table 7 and Table 8. The first column is the corresponding kinetic parameters for the reactions in the bond graph where the subscript is the reaction number. The original units in Parent et al. (1992) were $mole^{-2}.s^{-1}$, $mole^{-1}.s^{-1}$ or s^{-1} , while the units were changed to $M^{-2}.s^{-1}$, $M^{-1}.s^{-1}$ or s^{-1} in Eskandari et al. (2005) where the model (Parent et al., 1992) was reused. We found that using the units in Eskandari et al. (2005) gave the right dynamic outputs, so we used $M^{-2}.s^{-1}$, $M^{-1}.s^{-1}$ or s^{-1} in this article and the primary paper (Hunter et al., 2025).

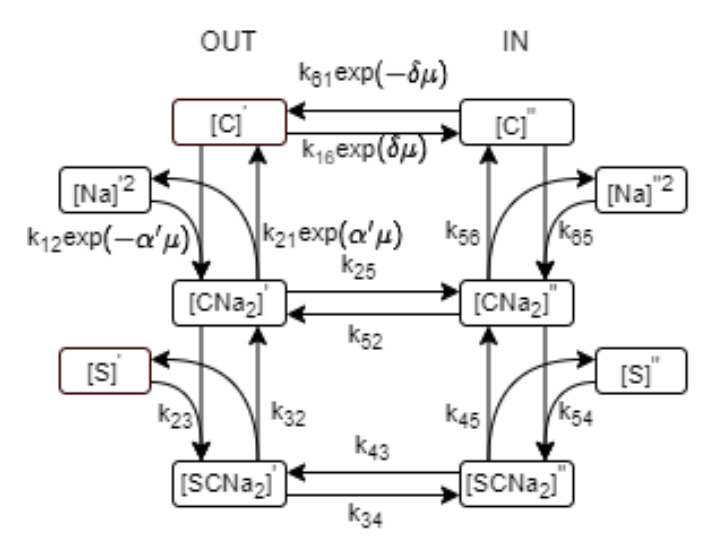


Figure 5. Kinetic model diagram adapted from Figure 1 of Parent et al. (1992). Note that the notations are different from the bond graph: $[C]' - E_o(BG); [C]'' - E_i(BG);$ $[CNa_2]' - E_o2Na^+(BG); [CNa_2]'' - E_i2Na^+(BG); [SCNa_2]' - E_o2Na^+Glc(BG);$ $[SCNa_2]'' - E_i2Na^+Glc(BG); [Na]' - Na_o(BG); [Na]'' - Na_i(BG); [S]' - Glc_o(BG);$ $[S]'' - Glc_i(BG)$. $\delta = 0.7$, $\alpha' = 0.3$ and we omitted the electrical field between [C]'' and $[CNa_2]''$ because $\alpha'' = 0$ in Parent et al. (1992). $\mu = \frac{FV}{RT}$ where V is the membrane potential, F = 96485C/mol and R = 8.314J/mol/K are Faraday constant and universal gas constant, respectively, and T = 293K is temperature. The letters associated with the edges are the rate constants and the arrows indicate the flux directions.

4.1 Bond graph parameters

We apply the same method (Pan, 2019) to convert the kinetic parameters to bond graph parameters. Since we have described how to link kinetic parameters to bond graph parameters in Section 3.1, we directly solve Equation 15 to get the bond graph parameters for SLC5A1 without repeating the derivation process. First, we construct matrices k^+ , k^- , N^f , N^r and W to get Equation 15 for SLC5A1. The vectors of the forward and reverse kinetic rate constants k^+ , k^- are defined below and the values are from Table 7 and Table 8.

$$\mathbf{k}^{+} = \begin{bmatrix} k_{1}^{+} \\ k_{2}^{+} \\ k_{3}^{+} \\ k_{4}^{+} \\ k_{5}^{+} \\ k_{6}^{+} \\ k_{7}^{+} \end{bmatrix}, \ \mathbf{k}^{-} = \begin{bmatrix} k_{1}^{-} \\ k_{2}^{-} \\ k_{3}^{-} \\ k_{3}^{-} \\ k_{5}^{-} \\ k_{6}^{-} \\ k_{7}^{-} \end{bmatrix}$$
(36)

Note that we do not need to add constraints therefore both K^c and N^c are empty in this case. The forward and reverse stoichiometric matrices (N^f , N^r) are shown in Table 9 and Table 10, respectively. The first row lists the reactions while the first column denotes the species.

Based on McLaren et al. (1987) we set the volume of blood cells to $V_i = 8.5 \times 10^{-2}$ (pL) and use the same value for the extracellular volume. The diagonal matrix **W** that accounts for the volumes of compartments is constructed in Equation 37.

Note that when preparing this Physiome manuscript we discovered a unit conversion error of the cell volume used to calculate parameter values in the Primary paper (Hunter et al., 2025). This error scaled up the thermodynamical parameters of Na and Glc by 10^7 , i.e., K_i^{Na} , K_o^{Na} , K_i^{Glc} and K_o^{Glc}

Table 7. The kinetic parameters for simulation of Fig. 10 in Parent et al. (1992).

Kinetic in BG	Parameter	Value	Unit	Remark
	k ₁₂	80000	$M^{-2}.s^{-1}$	$8 \times 10^4 \times 10^{-6} \ (mM^{-2}.s^{-1})$
k_2^+	k ₂₃	1e5	$M^{-1}.s^{-1}$	$1 \times 10^5 \times 10^{-3} \ (mM^{-1}.s^{-1})$
k_2^{+}	k ₃₄	50	s^{-1}	
k_{A}^{+}	k ₄₅	800	s^{-1}	
k_5^{+}	k ₅₆	10	s^{-1}	
k_6^+	k ₆₁	5	s^{-1}	
k_7^+	k ₂₅	0.3	s^{-1}	
$k_1^{'-}$	k ₂₁	500	s^{-1}	
k_2^{-}	k ₃₂	20	s^{-1}	
$k_3^{\frac{2}{-}}$	k ₄₃	50	s^{-1}	
k_{\perp}^{-}	k ₅₄	1.8285e7 ¹	$M^{-1}.s^{-1}$	$1.8285e7 \times 10^{-3} \ (mM^{-1}.s^{-1})$
$k_5^{\frac{1}{2}}$	k ₆₅	50	$M^{-2}.s^{-1}$	$50 \times 10^{-6} \ (mM^{-2}.s^{-1})$
k_6^{-}	k ₁₆	35	s^{-1}	
k_{1}^{+} k_{2}^{+} k_{3}^{+} k_{4}^{+} k_{5}^{+} k_{6}^{+} k_{1}^{-} k_{2}^{-} k_{3}^{-} k_{4}^{-} k_{5}^{-} k_{6}^{-} k_{7}^{-}	k ₅₂	1.371 ²	s^{-1}	

Table 8. The kinetic parameters for simulation of Fig. 5 in Parent et al. (1992).

Kinetic in BG	Parameter	Value	Unit	Remark
${k_{1}^{+}}$	k ₁₂	80000	$M^{-2}.s^{-1}$	$8 \times 10^4 \times 10^{-6} \ (mM^{-2}.s^{-1})$
k_2^+	k ₂₃	1e5	$M^{-1}.s^{-1}$	$1 \times 10^5 \times 10^{-3} \ (mM^{-1}.s^{-1})$
$k_3^{\frac{2}{+}}$	k ₃₄	50	s^{-1}	
k_{4}^{+}	k ₄₅	800	s^{-1}	
k_{5}^{4}	k ₅₆	10	s^{-1}	
$egin{array}{c} k_1^+ & k_2^+ & k_3^+ & k_4^+ & k_5^+ & k_6^+ & k_7^- & k_2^- & k_3^- & k_5^- & k_6^- & k_7^- & k_8^- & k_7^- & k_8^- & k_7^- & k_8^- & k_7^- & k_8^- & k_8^$	k ₆₁	3	s^{-1}	
k_7^+	k ₂₅	0.3	s^{-1}	
$k_1^{\prime -}$	k ₂₁	500	s^{-1}	
k_2^{\perp}	k ₃₂	20	s^{-1}	
k_{3}^{2}	k ₄₃	50	s^{-1}	
k_{Δ}^{-}	k ₅₄	1.0971e7 ¹	$M^{-1}.s^{-1}$	$1.0971e7 \times 10^{-3} \ (mM^{-1}.s^{-1})$
k_5^{-}	k ₆₅	50	$M^{-2}.s^{-1}$	$50 \times 10^{-6} \ (mM^{-2}.s^{-1})$
k_6^-	k ₁₆	35	s^{-1}	
k_7^-	k ₅₂	0.823 ²	s^{-1}	

Table 9. Forward stoichiometric matrix N^f for the SLC5A1.

	Re ₁	Re ₂	R e ₃	Re ₄	R e ₅	Re ₆	Re ₇
Nai	0	0	0	0	0	0	0
Nao	2	0	0	0	0	0	0
Glci	0	0	0	0	0	0	0
Glco	0	1	0	0	0	0	0
1	1	0	0	0	0	0	0
2	0	1	0	0	0	0	1
3	0	0	1	0	0	0	0
4	0	0	0	1	0	0	0
5	0	0	0	0	1	0	0
6	0	0	0	0	0	1	0

¹ k_{54} is calculated by the detailed balance equations $k_{54} = k_{23} * k_{34} * k_{45} * k_{52}/(k_{32} * k_{43} * k_{25})$.
² k_{52} is calculated by the detailed balance equations $k_{52} = k_{12} * k_{25} * k_{56} * k_{61}/(k_{21} * k_{65} * k_{16})$.

¹ k_{54} is calculated by the detailed balance equations $k_{54} = k_{23} * k_{34} * k_{45} * k_{52}/(k_{32} * k_{43} * k_{25})$. ² k_{52} is calculated by the detailed balance equations $k_{52} = k_{12} * k_{25} * k_{56} * k_{61}/(k_{21} * k_{65} * k_{16})$.

Table 10. Reverse stoichiometric matrix N^r for the SLC5A1.

	Re ₁	Re ₂	<i>Re</i> ₃	Re ₄	Re ₅	Re ₆	Re ₇
Nai	0	0	0	0	2	0	0
Nao	0	0	0	0	0	0	0
Glci	0	0	0	1	0	0	0
Glco	0	0	0	0	0	0	0
1	0	0	0	0	0	1	0
2	1	0	0	0	0	0	0
3	0	1	0	0	0	0	0
4	0	0	1	0	0	0	0
5	0	0	0	1	0	0	1
6	0	0	0	0	1	0	0

with corrected values given in Tables 11, 12 and 13. Since the product of the thermodynamical parameter and cell volume, e.g., $K_i^{Na}V_i$, determines the dynamics of the system, the scaling effect $(K_i^{Na} \cdot 10^7 \cdot V_i \cdot 10^{-7})$ is canceled. Therefore, this change does not affect the model dynamics or simulation results.

Given that we have constructed all the matrices needed in Equation 15, we now apply the method in Equation 19 to obtain the bond graph parameters for SLC5A1, which are shown in Table 11 and Table 12.

Equations 37 and 38 in Hunter et al. (2025) gave the steady-state flux under the assumption that binding and unbinding occur very rapidly in comparison with the transition rates for the carrier protein. We arbitrarily set high values of reaction rate constants to reflect the fast binding and unbinding assumptions, and the parameters are shown in Table 13.

Figure 6 shows the steady-state fluxes from the bond graph model (encoded in $SGLT1_BG_fast.cellml$) and steady-state models (encoded in $SGLT1_ss_fast.cellml$) using the parameters in Table 13, which confirms that the analytic steady-state equations 37 and 38 is a good approximation of the full bond graph model when the fast binding and unbinding assumption holds, and the slippage (reaction Re_7 in Figure 4) is negligible.

To get the steady state flux from the full bond graph </Electrogenic cotransporter/SGLT1_BG_fast.cellml>, we need to use OpenCOR to manually run each simulation and export the required output variables. The SED-ML file </Electrogenic cotransporter/SGLT1_BG_fast.sedml> provides the required

Table 11. The bond graph parameters of the full BG model for SLC5A1 corresponding to Fig.10 of Parent et al. (1992) .

Parameter	Value	Units
<i>κ</i> ₁	47.906	fmol. s^{-1}
κ_2	2.325	fmol. s^{-1}
K 3	5.813	fmol. s^{-1}
κ_4	93.002	fmol. s^{-1}
K 5	0.21	fmol. s^{-1}
K 6	15.66	fmol. s^{-1}
K 7	0.029	fmol. s^{-1}
K_i^{Na}	0.322	$fmol^{-1}$
K _i K _o Na K _i GIc K _o GIc	0.322	$fmol^{-1}$
K_i^{Glc}	48.5	$fmol^{-1}$
$K_{o}^{'GIc}$	48.5	$fmol^{-1}$
K_1	2.235	$fmol^{-1}$
K_2	10.437	$fmol^{-1}$
<i>K</i> ₃	8.602	$fmol^{-1}$
K_4	8.602	$fmol^{-1}$
K_5	47.713	$fmol^{-1}$
<i>K</i> ₆	0.319	$fmol^{-1}$

Table 12. The bond graph parameters of the full BG model for SLC5A1 corresponding to Fig.5 of Parent et al. (1992) .

Parameter	Value	Unit		
κ ₁	47.905	$f mol.s^{-1}$		
κ_2	2.325	$fmol.s^{-1}$		
κ_3	5.812	$f mol.s^{-1}$		
κ_4	92.998	$f mol.s^{-1}$		
K 5	0.349	$f mol.s^{-1}$		
K 6	15.661	$f mol.s^{-1}$		
K 7	0.029	$f mol.s^{-1}$ $f mol^{-1}$ $f mol^{-1}$		
K_i^{Na}	0.322			
$K_o^{'Na}$	0.322			
K_i^{Glc}	48.5	$f mol^{-1}$		
K _i K _o GIc	48.5	$f mol^{-1}$		
K_1	2.235	$f mol^{-1}$		
K_2	10.437	$f mol^{-1}$		
K_3	8.602	$f mol^{-1}$		
K_4	8.602	$f mol^{-1}$		
K_5	28.628	$f mol^{-1}$		
<i>K</i> ₆	0.192	$f mol^{-1}$		

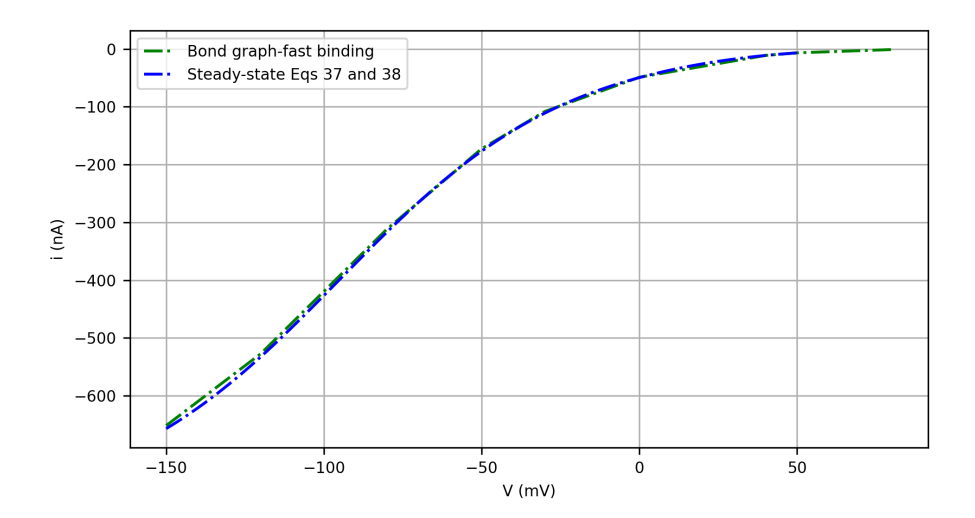


Figure 6. The steady-state results predicted by the full bond graph model, compared with the results from the reduced steady-state model. Both simulations use the assumption of fast binding/unbinding. This is Figure 10 in Hunter et al. (2025).

simulation settings. For each simulation, the readers need to modify the test potential (variable $test_volt$ in the component run_SGLT1_BG) to one of the values -0.15, -0.12, -0.08, -0.05, -0.03, 0, 0.04, 0.05, 0.08 (V), and the extracellular glucose concentration (variable Glco in the component run_SGLT1_BG) to 1e-12 (mM) or 1 (mM) for before and after addition of glucose, respectively.

The variables to export are VO_Vm and Ii in the component $SGLT1_BG$. For the Python script $mergeData_SGLT1.py$ in the src folder to process the data, readers must export the simulation data as a CSV file and follow a specific format when naming these files. The string indicating the experiment is $SGLT1_BG_step_ss_fast_Data$, followed by the glucose condition and the test potential in mV.

For example, $SGLT1_BG_step_ss_fast_Data_sugar_m50mV.csv$ denotes the test potential is $-50 \, (mV)$ and extracellular glucose concentration is $1 \, (mM)$, while $SGLT1_BG_step_ss_fast_Data_50mV.csv$ indicates the test potential is $50 \, (mV)$ and extracellular glucose concentration is $1e-12 \, (mM)$ (no sugar present in the filename). Under default conditions, the Ii value should be approximately $5,658,461.44 \, fA$ at the end of the simulation, while Ii equals $399,880.12 \, fA$ when $test_volt$ is set to $0 \, V$. Please note that the value may vary slightly due to numerical solving errors on different computers.

We have provided the data in <Electrogenic cotransporter\CellMLV2\sim_results>. The simulation protocol and the calculation process for the I-V curve are the same as for Fig. 5 in Parent et al. (1992), which will be detailed in the following section.

4.2 Simulation results

We followed the experiment conditions in Parent et al. (1992) to simulate the time course of the carrier-mediated currents (Fig.10 in Parent et al. (1992)) and the steady-state glucose-dependent I-V curve (Fig.5 in Parent et al. (1992)). The experiment conditions for Fig. 5 and Fig. 10 in Parent et al. (1992) are summarized in Table 14.

We use the parameters in Table 11 with the experiment conditions specified in Table 14 to simulate the time course of the carrier-mediated currents of the bond graph model as shown in Figure 7.

A pulse protocol is applied. The holding potential is $-50 \, (mV)$, and at time $t=4.75 \, (ms)$, the potential was stepped to the test potential for $80 \, (ms)$ (Parent et al., 1992). The test potentials are

 $\textbf{Table 13.} \ \ \textbf{The bond graph parameters for SLC5A1 with the fast binding/unbinding assumption.}$

Parameter	Value	Unit		
κ ₁	1.52E+04 f mol.s			
κ_2	6.24E+02	$fmol.s^{-1}$		
K 3	0.156	$fmol.s^{-1}$		
κ_4	2.50E+04	$fmol.s^{-1}$		
K 5	1.11E+02	$f mol.s^{-1}$		
K 6	9.562	$f mol.s^{-1}$		
K 7	9.09E-04	$f mol.s^{-1}$		
K_i^{Na}	1.41	$f mol^{-1}$		
K_i^{Na} K_o^{O}	1.41	$f mol^{-1}$		
K ^{Ğlc} K ^{Glc}	57.2	$f mol^{-1}$		
K_o^{GIc}	57.2	$f mol^{-1}$		
K_1	3.66	$f mol^{-1}$		
K_2	3.30E+02	$f mol^{-1}$		
K_3	3.21E+02	$f mol^{-1}$		
K_4	3.21E+02	$f mol^{-1}$		
K_5	9.05E+02	$f mol^{-1}$		
K_6	0.314	$f mol^{-1}$		

Table 14. The experiment conditions in Fig.5 and Fig. 10 of Parent et al. (1992).

Variable	Meaning	Value	Unit	Fig #	Remark
$[Na^+]_i$	intracellular <i>Na</i> ⁺ concentration	20	mM	Fig.5, Fig.10	$q_i^{Na} = [Na^+]_i \times V_i$
$[Na^+]_o$	extracellular <i>Na</i> ⁺ concentration	100	mM	Fig.5, Fig.10	$q_o^{Na} = [Na^+]_o \times V_o$
$[\alpha MDG]_i$	intracellular glucose concentration	10e-3	mM	Fig.5, Fig.10	$\begin{vmatrix} q_i^{GIc} = [\alpha MDG]_i \times \\ V_i \end{vmatrix}$
[αMDG] _o	extracellular glucose concentration	0	mM	Fig.5, Fig.10 without glucose	$q_o^{GIc} = [\alpha MDG]_o \times V_o$
[αMDG] _o	extracellular glucose concentration	1	mM	Fig.5, Fig.10 with glucose	$q_o^{G/c} = [\alpha MDG]_o \times V_o$
C_T	the number of trans- porters per oocyte	6×10 ¹⁰		Fig.5, Fig.10	$q_{tot} = \frac{C_T}{6.022 \times 10^{23}} \times 10^{15}$
hold _{volt}	Holding potential	-50	mV	Fig.5, Fig.10	
test _{volt}	Test potential	50 and -150	mV	Fig.10	More values for Fig. 5.

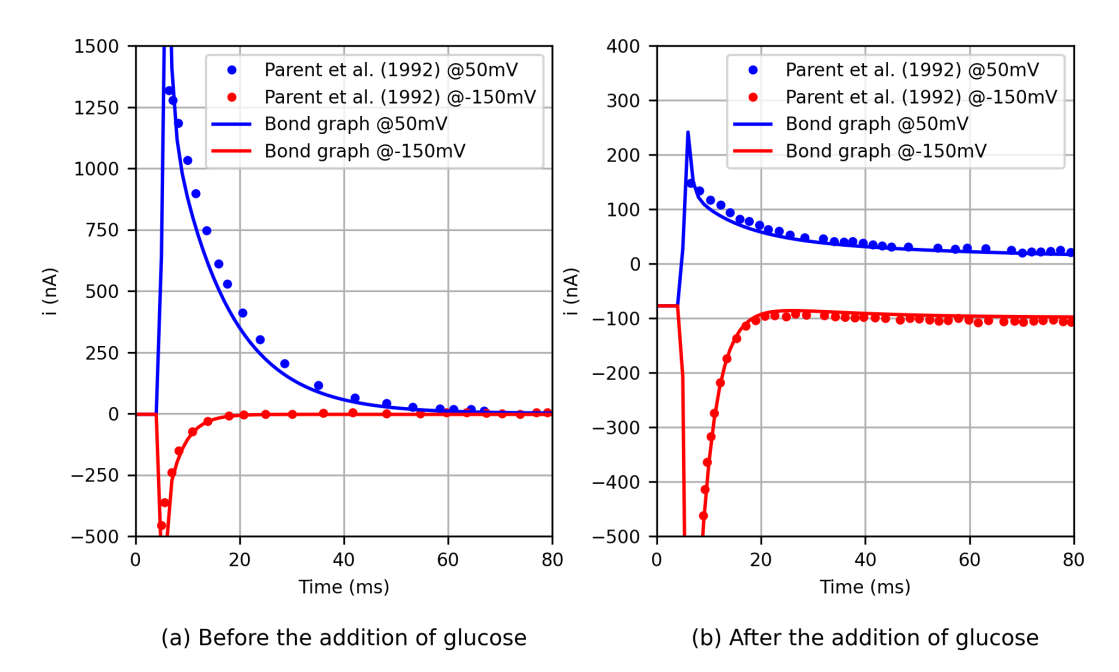


Figure 7. The time course of the carrier-mediated currents. (a) The electrical current when $[Glc]_o = 0 \ (mM)$, and (b) the current when $[Glc]_o = 1 \ (mM)$; The output of the bond graph model is the current $-I_i$, and the data of Parent et al. (1992) were derived using digitizing software Engauge (Mitchell et al., 2020) from Fig 10 (Parent et al., 1992). This is Figure 11 in Hunter et al. (2025).

 $50 \, (mV)$ and $-150 \, (mV)$ for upper plots and lower plots in Fig 10 (Parent et al., 1992), respectively. For the bond graph model, we applied the test potential at $t = 1204.75 \, (ms)$ to allow the system to reach steady-state. In Figure 7, we aligned the simulation traces with the data from Parent et al. (1992).

In the bond graph model (encoded in *SGLT1_BG.cellml*), the positive sign of $I_i = z_1 F v_1 + z_1 F v_1 + z_2 F v_6 + z_2 F v_6$ with $z_1 = 0.3$, $z_2 = 0.7$ indicates the current from extracellular to intracellular, while the direction of current in Parent et al. (1992) is from intracellular to extracellular. Hence, we show the model currents $-I_i$ before and after the addition of glucose in Figure 7.

To produce the steady-state glucose-dependent I-V curve in Fig 5 (Parent et al., 1992), we apply a range of test potentials including -150, -120, -80, -50, -30, 0, 40, 50, 80 (mV) and the parameters in Table 12. After the application of test potential at t=1.20475 (s), the current $-I_i$ at t=2.9845 (s) is saved as steady-state value. For each test potential, we simulated the steady-state current $-I_i$ under two conditions: before and after the addition of glucose (i.e., when $\lceil \alpha MDG \rceil_o = 0$ (mM) and $\lceil \alpha MDG \rceil_o = 1$ (mM). The glucose-dependent current was calculated using the difference in the current values $-I_i$ when $\lceil \alpha MDG \rceil_o = 1$ (mM) and $\lceil \alpha MDG \rceil_o = 0$ (mM). The bond graph simulated result is shown in red plot in Figure 8. The data from Parent et al. (1992) were derived using digitizing software Engauge (Mitchell et al., 2020).

We have provided the Python scripts under the folder <src> to run the simulations and plot the data, while the SED-ML files in <Electrogenic cotransporter\CellMLV2> detail the simulation settings. To get the result in Figures 8 and 7, the Python scripts $sim_SGLT1.py$, $mergeData_SGLT1.py$, $plot_SGLT1.py$ should run in sequence.

5 Conclusion

We have provided here detailed information on the two exemplar models presented in Hunter et al. (2025) to demonstrate the application of the energy-based modelling framework. The derivation of the bond graph parameters has been shown and instructions on reproducing the simulation

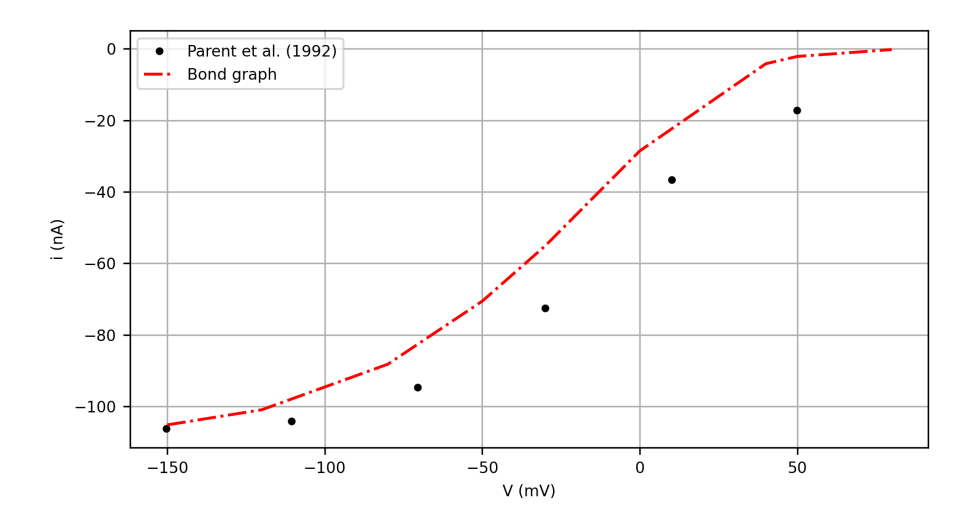
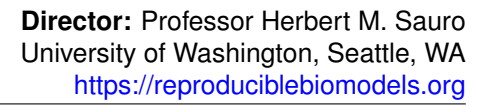


Figure 8. The steady-state glucose-dependent I-V curve of the full bond graph model compared with the data in Fig. 5 in Parent et al. (1992). This is Figure 12 in Hunter et al. (2025).

experiments presented in Hunter et al. (2025) provided. All the required model definition files and execution scripts are provided in the OMEX archive associated with this article.

References

- A. A. Cuellar, C. M. Lloyd, P. F. Nielsen, D. P. Bullivant, D. P. Nickerson, and P. J. Hunter. An overview of CellML 1.1, a biological model description language. *SIMULATION*, 79(12):740–747, 2003. URL https://doi.org/10.1177/0037549703040939.
- S. Eskandari, E. Wright, and D. Loo. Kinetics of the reverse mode of the Na+/glucose cotransporter. *The Journal of Membrane Biology*, 204:23–32, 2005.
- P. J. Hunter, W. Ai, and D. P. Nickerson. Energy-based bond graph models of glucose transport with SLC transporters. *Biophysical Journal*, 124(2):316–335, 2025. ISSN 0006-3495. doi: https://doi.org/10.1016/j.bpj.2024.12.006.
- A. G. Lowe and A. R. Walmsley. The kinetics of glucose transport in human red blood cells. *Biochimica et Biophysica Acta (BBA)-Biomembranes*, 857(2):146–154, 1986.
- C. E. McLaren, G. M. Brittenham, and V. Hasselblad. Statistical and graphical evaluation of erythrocyte volume distributions. *American Journal of Physiology-Heart and Circulatory Physiology*, 252(4):H857–H866, 1987.
- M. Mitchell, B. Muftakhidinov, T. Winchen, A. Wilms, B. v. Schaik, badshah400, Mo-Gul, T. G. Badger, Z. Jędrzejewski-Szmek, kensington, and kylesower. markummitchell/engauge-digitizer: Nonrelease, July 2020. URL https://doi.org/10.5281/zenodo.3941227.
- M. Pan. A bond graph approach to integrative biophysical modelling. PhD thesis, University of Melbourne, Parkville, Victoria, Australia, 2019.
- L. Parent, S. Supplisson, D. D. Loo, and E. M. Wright. Electrogenic properties of the cloned Na+/glucose cotransporter: II. A transport model under nonrapid equilibrium conditions. *The Journal of Membrane Biology*, 125:63–79, 1992.
- T. Yu, C. M. Lloyd, D. P. Nickerson, M. T. Cooling, A. K. Miller, A. Garny, J. R. Terkildsen, J. Lawson, R. D. Britten, P. J. Hunter, and P. M. F. Nielsen. The Physiome Model Repository 2. *Bioinformatics*, 27(5):743–744, 01 2011. ISSN 1367-4803. URL https://doi.org/10.1093/bioinformatics/btq723.





Reproducibility report for: Energy-based bond graph models of glucose transport with SLC transporters

Submitted to: Physiome

Manuscript identifier: S000029

Curation outcome summary: We successfully reproduced Figures 3a, 3b, 6, 7a and 8 as shown in the manuscript.

Box 1: Criteria for repeatability and reproducibility				
■ Model source code provided:				
■ Source code: a standard procedural language is used (e.g. MATLAB, Python, C)				
 There are details/documentation on how the source code was compiled There are details on how to run the code in the provided documentation The initial conditions are provided for each of the simulations Details for creating reported graphical results from the simulation results 				
■ Source code: a declarative language is used (e.g. SBML, CellML, NeuroML)				
 The algorithms used are defined or cited in previous articles The algorithm parameters are defined Post-processing of the results are described in sufficient detail 				
□ Executable model provided:				
\Box The model is executable without source (e.g. desktop application, compiled code, online service)				
\square There are sufficient details to repeat the required simulation experiments				
■ The model is described mathematically in the article(s):				
■ Equations representing the biological system				
■ There are tables or lists of parameter values				
■ There are tables or lists of initial conditions				
Machine-readable tables of parameter values				
■ Machine-readable tables of initial conditions				
■ The simulation experiments using the model are described mathematically in the article:				
■ Integration algorithms used are defined				
☐ Stochastic algorithms used are defined				
\square Random number generator algorithms used are defined				
\square Parameter fitting algorithms are defined				
$\hfill\Box$ The paper indicates how the algorithms yield the desired output				

CRBM Reproducibility Report version 1.3



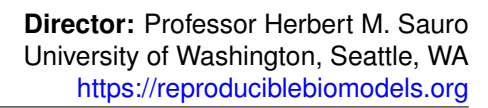
Box 2: Criteria for accessibility

- Model/source code is available at a public repository or researcher's web site
 - License provided
 - License is Open Source Initiative (OSI)-approved
- All simulation experiments are fully defined (events listed, collection times and measurements specified, algorithms provided, simulator specified, etc.)

Box 3: Evaluation

- Model and its simulations could be repeated using provided declarative or procedural code
- ☐ Model and its simulations could be reproduced

CRBM Reproducibility Report version 1.3





Summary comments: The model and source code were obtained from the link in the manuscript to the Physiome Model Repository. This was used together with the procedure described in the paper. We successfully reproduced Figures 3a, 3b, 6, 7a and 8 as shown in the manuscript, however, were unable to reproduce the "Bond graph @ -150mV" plot in Figure 7b. Additionally, the authors did not specify the Python version used in their simulation, so a best guess of Python 3.11.12 was used in our attempt to reproduce their plots.

Anand K. Rampadarath¹, PhD

Award Rampadasak

Curator at Center for Reproducible Biomedical Modeling

CRBM Reproducibility Report version 1.3

¹Contact: info@reproduciblebiomodels.org